Sentinel-1 TOPS interferometry for along-track displacement measurement

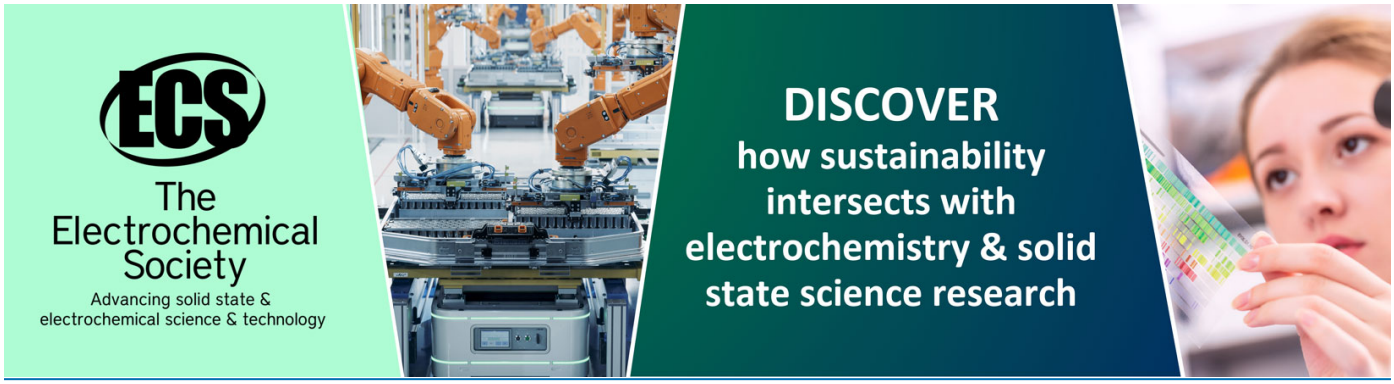

Sentinel-1 TOPS interferometry for along-track displacement measurement

H J Jiang[1], Y Y Pei[2] and J Li[1]

[1] School of Geographic and Biologic Information, Nanjing University of Posts and Telecommunications, Nanjing 210023, China
[2] School of Civil Engineering, Anhui Jianzhu University, Hefei 230601, China

jianghouj@njupt.edu.cn

Abstract. The European Space Agency's Sentinel-1 mission, a constellation of two C-band synthetic aperture radar (SAR) satellites, utilizes terrain observation by progressive scan (TOPS) antenna beam steering as its default operation mode to achieve wide-swath coverage and short revisit time. The beam steering during the TOPS acquisition provides a means to measure azimuth motion by using the phase difference between forward and backward looking interferograms within regions of burst overlap. Hence, there are two spectral diversity techniques for along-track displacement measurement, including multi-aperture interferometry (MAI) and "burst overlap interferometry". This paper analyses the measurement accuracies of MAI and burst overlap interferometry. Due to large spectral separation in the overlap region, burst overlap interferometry is a more sensitive measurement. We present a TOPS interferometry approach for along-track displacement measurement. The phase bias caused by azimuth miscoregistration is first estimated by burst overlap interferometry over stationary regions. After correcting the coregistration error, the MAI phase and the interferometric phase difference between burst overlaps are recalculated to obtain along-track displacements. We test the approach with Sentinel-1 TOPS interferometric data over the 2015 Mw 7.8 Nepal earthquake fault. The results prove the feasibility of our approach and show the potential of joint estimation of along-track displacement with burst overlap interferometry and MAI.

1. Introduction

Sentinel-1, the new generation of European Space Agency's (ESA) C-band synthetic aperture radar (SAR) mission, provides data continuity to its previous European Remote Sensing (ERS) and ENVISAT SAR missions [1]. The Sentinel-1 mission is comprised of two identical radar satellites to form a constellation, which can significantly reduce the revisit time.

Sentinel-1's SAR instrument supports four imaging modes providing different resolution and coverage: Interferometric Wide Swath Mode (IW), Extra Wide Swath Mode (EW), StripMap (SM), and Wave (WV). Terrain observation by progressive scan (TOPS) antenna beam steering is utilized for the IW mode to provide a 250 km wide swath consisting of three sub-swaths at 5 m × 20 m resolution [2]. Due to the wide swath, the revisit cycle has been notably reduced from 35 days for ERS-1 and ERS-2 or 30/35 days for ENVISAT to 12 days for Sentinel-1, and can be reduced to 6 days when the two satellites are in orbit. The IW mode based on TOPS is set as the default operation mode for Sentinel-1.

The TOPS acquisition can overcome the problems of scalloping and azimuth-varying signal-to-ambiguity ratio of the conventional ScanSAR mode by means of steering the antenna beam in the along-track direction [3]. The antenna beam is rotated throughout the acquisition from backward to

forward at a constant rotation rate, which leads to a reduction of the azimuth bandwidth, and consequently a worsening of the azimuth resolution. Since all targets are observed by the complete azimuth antenna pattern, the scalloping effect nearly eliminates, and the azimuth ambiguities and the signal-to-noise ratio become constant in azimuth. But the accuracy of along-track displacement measurement with multi-aperture interferometry (MAI) for Sentinel-1 IW mode will be much lower than that for SM mode, because its azimuth bandwidth and resolution are much lower than that of SM mode [2].

The MAI technique is an important complement to cross-track SAR interferometry (InSAR). A major limitation of InSAR for geophysical applications is that the technique is only sensitive to one dimensional motion along the satellite's line of sight (LOS), while measurements of the deformation field in three dimensions allow a better resolution of the parameters of deformation models for earthquakes, volcanic activity, and other processes. Therefore, the techniques for along-track displacement measurement should be fully exploited to improve the deformation resolving capability of Sentinel-1.

The antenna beam steering in TOPS acquisition provides another way for along-track displacement measurement. To assure that the images can be mosaiked without any gap, an overlap area is present in the azimuth direction between consecutive bursts. In the overlap area, the squint angle of the two consecutive bursts is changed from forward to backward, which results in a much larger azimuth spectral separation than the one achieved by MAI. Hence, the "burst overlap interferometry" gives a sensitive estimation for azimuth motion [4].

Both MAI and burst overlap interferometry have been used to estimate the azimuth coregistration error over stationary scenes [5]. This paper focuses on along-track displacement measurement using burst overlap interferometry and MAI with Sentinel-1 TOPS acquisitions over nonstationary scenes. A Sentinel-1 IW InSAR image pair over the 2015 Mw 7.8 Nepal earthquake fault is selected for demonstration.

2. Burst overlap interferometry and MAI

Burst overlap interferometry and MAI are spectral diversity techniques applied to the azimuth direction for along-track displacement measurement. The TOPS azimuth signal properties provide a probability for burst overlap interferometry, and require a deramping operation in interferometric processing steps. Table 1 lists the Sentinel-1 IW data parameters over the Nepal earthquake fault.

Table 1. Sentinel-1 IW data parameters over the 2015 Mw 7.8 Nepal earthquake fault

	sub-swath IW1	sub-swath IW2	sub-swath IW3
Incidence angle [deg]	34.66	39.93	44.48
Azimuth resolution [m]	22.5	22.7	22.6
Azimuth bandwidth [Hz]	327	313	314
Azimuth steering rate [deg/s]	1.59	0.98	1.40
Doppler rate [Hz/s]	-2265	-2129	-2000
Doppler centroid rate [Hz/s]	1745	1464	1539
$\Delta f_{DC}^{overlap}$ [Hz]	4813	4039	4245
Range bandwidth [MHz]	56.5	48.3	42.8
Azimuth sampling frequency [Hz]	486.49		
Azimuth spacing [m]	14		
Range sampling frequency [MHz]	64.35		
Range spacing [m]	2.3		
Wavelength [cm]	5.547		

2.1. Spectral Properties of TOPS azimuth signal

The properties of TOPS azimuth signal are a consequence of steering the antenna beam from backward to forward in azimuth direction, which produces a linear variation of the Doppler centroid frequency within each burst. The antenna beam steering introduces a Doppler centroid rate given by [3]

$$k_{rot} \approx -\frac{2v}{\lambda}\omega_r \tag{1}$$

where v is the satellite velocity, λ is the radar wavelength, and ω_r is the antenna beam steering rate.

After the raw data have been focused to SLC bursts in zero-Doppler geometry, a linear variation of Doppler centroid frequency is present in the azimuth direction. The new Doppler centroid rate in zero-Doppler geometry can be calculated as [3]

$$k_t = \frac{k_{rot} \cdot k_a}{k_a - k_{rot}} \tag{2}$$

where k_a is the Doppler rate.

Then the azimuth dependent Doppler centroid frequency can be written as

$$f_{DC} = k_t t_{az} \tag{3}$$

where t_{az} is the relative azimuth time within the burst. The Doppler variation has to be considered for interferometric processing, including spectral filtering and interpolation.

2.2. Accuracy analysis for burst overlap interferometry and MAI

Spectral diversity techniques measure along-track displacement by exploiting a differential interferogram obtained from two pairs of complex SAR images with an azimuth spectral separation. The phase of the differential interferogram is given by [6]

$$\phi_{sd} = 2\pi \cdot \Delta f \cdot x / ASF \tag{4}$$

where Δf is the spectral separation, x is the along-track displacement in units of resolution cells, and ASF is the azimuth sampling frequency.

According to equation (4), the Cramér-Rao bound in estimation of along-track displacement with MAI can be written in terms of standard deviation of resolution cells [5]

$$\sigma_{MA} = \frac{1}{2\pi\Delta f_{MA}}\sqrt{\frac{3}{N}}\frac{\sqrt{1-\gamma^2}}{\gamma}ASF \tag{5}$$

where Δf_{MA} is the spectral separation of the two sublooks, which is equal to 2/3 azimuth bandwidth when the accuracy approaches the Cramér-Rao bound, N is the number of independent averaged samples, and γ is the interferometric coherence.

Similarly, the estimation accuracy with burst overlap interferometry in terms of resolution cells is given by [5]

$$\sigma_{ovl} = \frac{1}{2\pi\Delta f_{ovl}}\frac{1}{\sqrt{N}}\frac{\sqrt{1-\gamma^2}}{\gamma}ASF \tag{6}$$

where Δf_{ovl} is the spectral separation in the burst overlap region.

As shown in table 1, Δf_{ovl} is over 20 times larger than Δf_{MA}. Usually the value of N for burst overlap interferometry is about 7% of that for MAI in Sentinel-1 IW case. Using equation (5), (6) and the parameters in table1 and taking all available pixels averaged, we find that the estimation accuracy of burst overlap interferometry is over 10 times better than that of MAI, since the accuracy improves inversely proportional to Δf, while only inversely proportional to the square root of N.

On the other hand, large spectral separation will wrap the phase ϕ_{sd}, and reduce the maximum displacement x_{max} that can be measured without ambiguity. x_{max} is given by

$$x_{\max} = \pm \frac{1}{2\Delta f} ASF \tag{7}$$

This value is equal to ±1.147 pixels for MAI and ±0.056 pixels for burst overlap interferometry with three sub-swaths IW1, IW2 and IW3 in average, using $\Delta f_{MA} = 2B_{az}/3$ (B_{az}: azimuth bandwidth) and the parameters in table 1.

2.3. Processing Strategy

The proposed approach with burst overlap interferometry and MAI for along-track displacement measurement involves the following steps:

- Coregistering the Sentinel-1 IW interferometric pair by using the precise orbit information and an external digital elevation model (DEM), such as an SRTM DEM. This geometric coregistration can achieve very good relative accuracy, both in range and azimuth dimensions. Therefore, only a constant coregistration offset remains, imposed by the limited orbit accuracy.
- Deramping the full resolution master and slave SLC images by the azimuth-variant Doppler centroid function equation (3) before cross-correlation coregistration, spectral filtering and interpolation. The consideration of the Doppler centroid frequency of the focused SLC burst is critical for interferometric processing.
- Refining the offsets obtained from geometric coregistration. The azimuth coregistration error, which will introduce an undesirable phase bias for along-track displacement measurement, is estimated by using equation (8). Regarding the range direction, cross-correlation is applied to patches distributed over the master and slave images and a linear correction of the shifts is performed.

$$x_{az} = \arg\min \left\{ \left| \arg \sum_i \gamma_i e^{j\left(\phi_{ovl,i} - 2\pi \Delta f_{ovl} \Delta x_{az} / ASF\right)} \right| \right\} \tag{8}$$

  where x_{az} is the azimuth coregistration error in units of resolution cells, ϕ_{ovl} is the interferometric phase difference between burst overlaps.
- Calculating the phase bias caused by the azimuth coregistration error for burst overlap interferometry and MAI using equation (4). The phase bias is then subtracted from the differential interferogram obtained from burst overlap interferometry and MAI.

3. Experimental results

The proposed approach is tested on a Sentinel-1 IW InSAR image pair over the 2015 Mw 7.8 Nepal earthquake fault. The image pair was acquired on 17 and 29 April 2015 in descending path 19. As shown in figure 1, The 250 km wide swath consists of three sub-swaths, covering the Himalayan Mountain and the Indo-Gangetic Plain.

The earthquake occurred on 25 April 2015 at a depth of approximately 8.2 km, with its epicentre (the red star in figure 1) approximately 80 km to the northwest of the Nepalese capital of Kathmandu [7]. The intensity contours in figure 1 portrays the distribution and severity of shaking. We can see that strong shakes are located at the top half of swath IW1 and IW2, which means ground displacements are present in this region. Therefore, the bursts over this region should be treated as nonstationary scenes.

The image pair is first coregistered using a geometrical approach. The image offsets are calculated with an SRTM DEM and the precise orbit state vectors. The precise orbit product has a 3D 1σ accuracy of 5 cm, which would turn into an azimuth error of 0.0036 pixels with an azimuth spacing of 14 m. This error is less than 1/10 of the ambiguity band of burst overlap interferometry as discussed in 2.2. Therefore the estimation of the azimuth coregistration error is not aliasing over stationary scenes when using burst overlap interferometry.

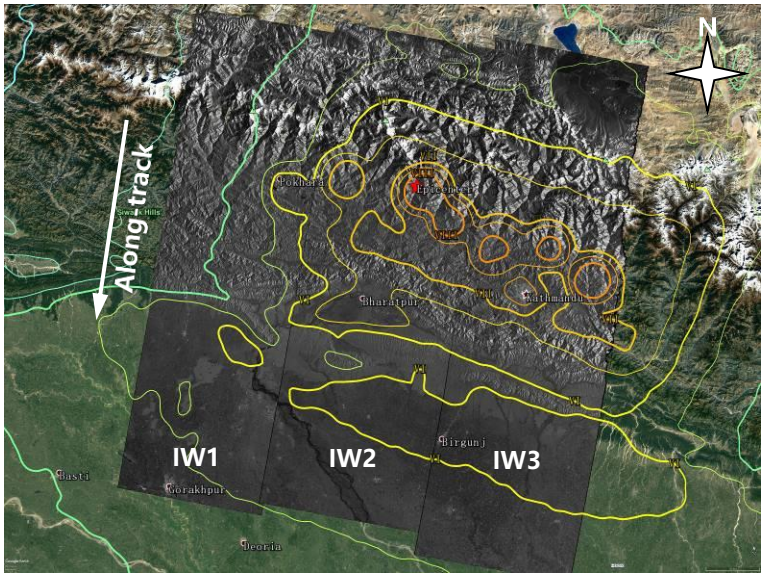

Figure 1. The Sentinel-1 IW detected SAR image over the 2015 Mw 7.8 Nepal earthquake fault. The red star marks the location of epicentre, and the coloured lines are the intensity contours of the earthquake published by USGS.

After the geometric coregistration, the full resolution master and slave SLC images are deramped to remove the phase ramp introduced by azimuth variation of Doppler centroid frequency. The image pair is then re-coregistered using cross-correlation to refine the range offsets, and the slave SLC image is resampled into the master image geometry. An interferogram is formed with the coregistered SLC images for burst overlap interferometry and LOS displacement measurement, and the phase ϕ_{ovl} is obtained from the differential interferograms within burst overlap regions. Meanwhile, the azimuth spectrums of the coregistered SLC images are filtered into two nonoverlapping bands with a spectral separation of $2B_{az}/3$, resulting in two pairs of sublook images for MAI.

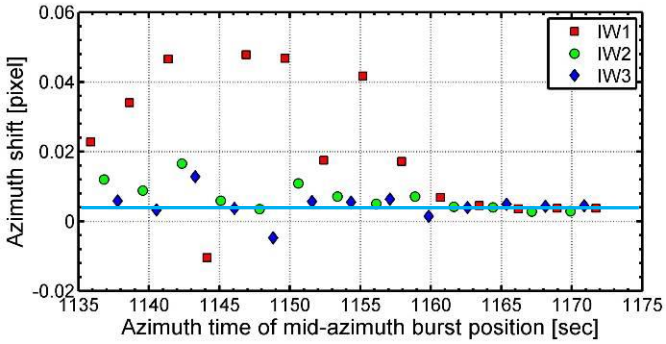

Figure 2. The azimuth shift estimated by using burst overlap interferometry. The cyan line indicates the average azimuth coregistration error of IW 1, IW2 and IW3.

The azimuth coregistration error is estimated using equation (8) over stationary regions. The results are plotted in figure 2. Each burst overlap region can give an estimate, and obviously the estimates close to the cyan line in figure 2 are related to the coregistration error, because the error should be nearly constant within each subswath after geo-metric coregistration. The estimated error of each subswath is 0.0038 pixels for IW1, 0.0035 pixels for IW2 and 0.0044 pixels for IW3. The average error of the three subswaths is about 5.5 cm, which is close to the accuracy of the precise orbit.

The estimates deviating from the cyan line in figure 2 are resulted from along-track displacement. After removing the azimuth coregistration error, the phase ϕ_{ovl} can represent the along-track displacement. The MAI interferogram is formed at last by a differential operation between the interferograms from the two pairs of sublook images. The phase bias due to the coregistration error is also corrected using equation (4).

Figure 3 and 4 portray the results of burst overlap interferometry and MAI respectively. It is observed that the along-track displacements mainly occur at the earthquake fault, and the displacement magnitude increases toward the centre of the fault rupture plane (the white quadrangle in figure 3 and 4). The result from burst overlap interferometry is more sensitive to along-track displacement compared with that from MAI. Note that the phase ϕ_{ovl} is wrapped over the fault rupture plane. Since ϕ_{ovl} is not continuous in azimuth direction, phase unwrapping should be carefully applied for further modelling of the deformation. Although the MAI result is less sensitive, the MAI phase is easier to unwrap, and is available over the whole image unless a strong decorrelation occurs. A combination of these two results may improve the modelling accuracy of the deformation.

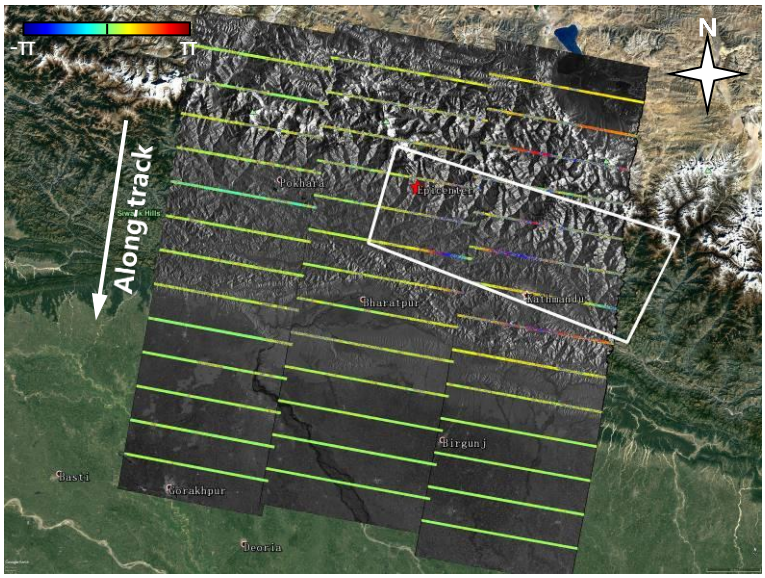

Figure 3. The differential interferogram in burst overlap regions. The red star is the epicentre, and quadrangle represents the approximate surface projection of the fault rupture plane.

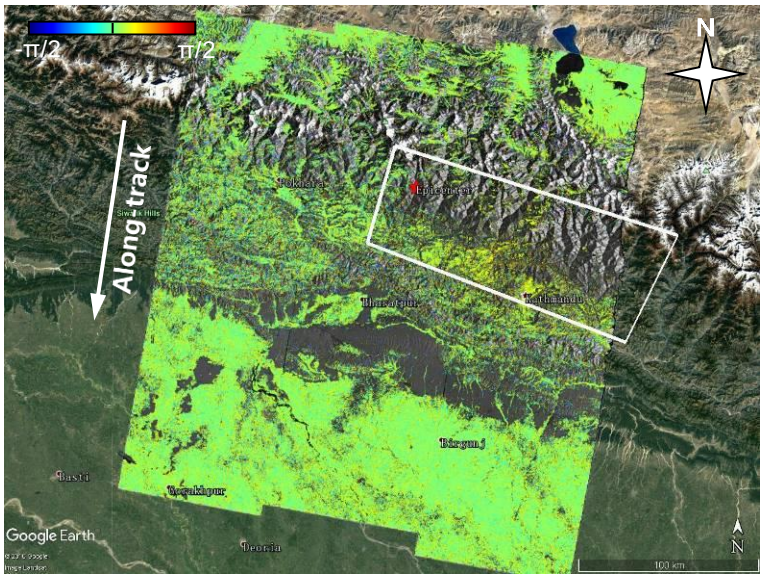

Figure 4. The MAI interferogram. The red star is the epicentre, and quadrangle represents the approximate surface projection of the fault rupture plane.

4. Conclusions

We analyze the accuracy of burst overlap interferometry and MAI for along-track displacement measurement in Sentinel-1 TOPS mode. We propose a data processing strategy to achieve very high accuracy of coregistration and to remove phase bias from the results of burst overlap interferometry and MAI. The approach is applied on Sentinel-1 TOPS interferometric data over the 2015 Nepal earthquake fault. The results prove that burst overlap interferometry is a more sensitive measurement, and a better deformation model might be built using a joint estimation with burst overlap interferometry and MAI.

Acknowledgments

This work was financially supported by the National Natural Science Foundation of China (Grant No. 41501497) and NUPTSF (Grant No. NY214197). The authors thank the European Space Agency for providing the Sentinel-1 A data.

References

[1] Salvi S, Stramondo S, Funning G J, Ferretti A, Sarti F and Mouratidis A 2012 The Sentinel-1 mission for the improvement of the scientific understanding and the operational monitoring of the seismic cycle *Remote Sensing of Environment* **120** 164-74

[2] Jung H S, Lu Z and Zhang L 2013 Feasibility of along-track displacement measurement from Sentinel-1 interferometric wide-swath mode *IEEE Transactions on Geoscience and Remote Sensing* **51** 573-8

[3] Zan F D and Guarnieri A M 2006 TOPSAR: terrain observation by progressive scans *IEEE Transactions on Geoscience and Remote Sensing* **44** 2352-60

[4] Scheiber R, Jäger M, Prats-Iraola P, Zan F D and Geudtner D 2015 Speckle tracking and interferometric processing of TerraSAR-X TOPS data for mapping nonstationary scenarios *IEEE Journal of Selected Topics in Applied Earth Observations and Remote Sensing* **8** 1709-20

[5] Prats-Iraola P, Scheiber R, Marotti L, Wollstadt S and Reigber A 2012 TOPS interferometry with TerraSAR-X *IEEE Transactions on Geoscience and Remote Sensing* **50** 3179-88

[6] Scheiber R and Moreira A, 2000 Coregistration of interferometric SAR images using spectral diversity *IEEE Transactions on Geoscience and Remote Sensing* **38** 2179-91

[7] Avouac J P, Meng L S, Wei S J, Wang T and Ampuero J P 2015 Lower edge of locked Main Himalayan Thrust unzipped by the 2015 Gorkha earthquake *Nature Geoscience* **8** 708-11